

Femtosecond laser damage of germanium from near- to mid-infrared wavelengths

Drake R. Austin,¹ Kyle R. P. Kafka,^{1,2}  Yu Hang Lai,¹ Zhou Wang,¹ Cosmin I. Blaga,¹ and Enam A. Chowdhury^{1,*}

¹Department of Physics, The Ohio State University, 191 West Woodruff Ave, Columbus, Ohio 43210, USA

²Laboratory for Laser Energetics, University of Rochester, Rochester, New York 14636, USA

*Corresponding author: chowdhury.24@osu.edu

Received 6 June 2018; revised 5 July 2018; accepted 5 July 2018; posted 6 July 2018 (Doc. ID 331769); published 27 July 2018

Femtosecond laser-induced damage and ablation (fs-LIDA) is a rich field in extreme non-perturbative nonlinear optics with wide ranging applications, including laser micro- and nano-machining, waveguide writing, and eye surgery. Our understanding of fs-LIDA, however, is limited mostly to visible and near-infrared wavelengths. In this work, we systematically study single-shot, fs-laser ablation (fs-LIA) of single-crystal germanium from near- to mid-infrared wavelengths, and compare the fs-LIA wavelength scaling with two widely used models. We show that these models are inadequate, particularly at mid-infrared wavelengths. Instead, a hybrid model is proposed involving Keldysh ionization rates, a constant free-carrier density threshold, and multi-band effects, which yields good agreement with experimental observations. Aspects of this model may be applied to understanding other strong-field non-perturbative phenomena in solids. © 2018 Optical Society of America

OCIS codes: (140.3070) Infrared and far-infrared lasers; (140.3330) Laser damage; (160.6000) Semiconductor materials; (320.2250) Femtosecond phenomena.

<https://doi.org/10.1364/OL.43.003702>

With the advancement of ultra-short pulse laser sources in mid- to far-infrared (IR) regimes [1–3], studies of nonlinear optical effects on IR materials have become very important [4,5]. With its transparency from 1.9 μm to 15 μm and its large third-order susceptibility ($\chi^{(3)}$), Ge is one of the most significant IR materials available with a wide range of applications [6,7], making laser-induced damage and ablation (LIDA) studies of Ge extremely important from an applications perspective. At mid- to far-IR wavelengths, various potential applications of Ge include the demonstration of plasmonic resonance activation with picosecond control [8] and the detection of trace amounts of chemically and biologically sensitive molecules through vibrational and rotational resonances in the so-called “molecular fingerprinting” region [9,10]. Furthermore, Ge photonic structures, such as buried waveguides written by mid-IR (MIR) lasers, could be useful in creating integrated optoelectronic chips using Si-based semiconductor industry architectures. The fabrication

of such structures has already been demonstrated in Si with MIR, femtosecond (fs) laser pulses [11].

The wavelength scaling of fs-LIDA is a very interesting way to study the physics of the damage process, because it not only allows testing of the validity of existing theoretical models of fs-LIDA, but may also lead to the discovery of novel non-perturbative behavior in laser–solid interactions. For example, exposing a semiconductor such as Ge to MIR, fs laser pulses open different paradigms of intense field light–matter interaction. First, the interaction range renders Ge from a highly absorptive material to a highly transparent one, as two-photon absorption dominates at wavelengths longer than $\sim 1.85 \mu\text{m}$ (indirect band gap $E_g = 0.67 \text{ eV}$ at room temperature). Second, with increasing wavelength, different considerations tend to predict different trends in laser damage. For example, if the onset of material damage is determined by the excitation of free-carriers to the critical plasma density N_{crit} , then the fs-LIDA threshold should exhibit a general decreasing trend with the laser wavelength λ , as N_{crit} scales proportionally with λ^{-2} . On the other hand, if fs-LIDA is determined by the energy density of excited electrons within the two-temperature model [12], then the ultra-short pulse fs-LIDA threshold should scale linearly with λ for all materials, as the pulse energy is distributed over a larger skin depth [13]. So far, very few experiments [14–16] have been performed to study the wavelength scaling of fs-LIDA. Reference [14] studied LIDA in the regime of picosecond pulses at $\lambda = 0.4\text{--}0.8 \mu\text{m}$ and $\lambda = 4.6\text{--}7.8 \mu\text{m}$. Among the only three previous published studies known on fs-LIDA of Ge, [17] and [18] concentrate on pump-probe studies at near-IR (NIR) ($\lambda = 0.8 \mu\text{m}$) and visible ($\lambda = 0.62 \mu\text{m}$) wavelengths, respectively, and [19] reports multi-pulse fs-LIDA at $\lambda = 3.9 \mu\text{m}$. It should be noted that since single pulse fs-LIDA almost always is due to an ultrafast phase change (i.e., ultrafast melting), which usually causes surface atomic layers to be ejected, fs laser damage and ablation are considered together more often than not.

In this Letter, the first results on the ultrashort, single-pulse laser-induced ablation (material removal from surface) thresholds of Ge at NIR and MIR wavelengths are presented, along with theoretical model predictions as benchmarks against the data. A multi-band model is introduced, which yields fairly

good agreement with experimental results. Such a model not only has relevance in fs-LID, but also in other strong-field, MIR phenomena involving electronic transitions between valence and conduction bands, such as high harmonic generation in solids [20] and plasmonic resonance excitations [9].

The samples used in this experiment were $1\text{ cm} \times 1\text{ cm}$, (100) plane, single-crystal, undoped Ge squares (MTI crystal) with a resistivity of $30\ \Omega \cdot \text{cm}$ and the principal planes oriented along the edges. The sample was oriented with the (110) direction aligned with the laser polarization (45° with respect to the edges). The native oxide was not removed from the sample surface. Experiments were carried out at wavelengths of $0.78\ \mu\text{m}$, $2.0\ \mu\text{m}$, $2.4\ \mu\text{m}$, $3.0\ \mu\text{m}$, and $3.6\ \mu\text{m}$ with respective pulse durations of 70 fs, 90 fs, 100 fs, 90 fs, and 90 fs and FWHM focal spot sizes $32\ \mu\text{m}$, $26\ \mu\text{m}$, $38\ \mu\text{m}$, $39\ \mu\text{m}$, and $43\ \mu\text{m}$ (geometric mean of horizontal and vertical spot sizes) using four separate laser systems including three optical parametric amplifiers (OPAs). The *s*- or *p*-polarized pulses were focused onto the sample at a 45° angle of incidence (chosen to probe whether the E-field orientation w.r.t. sample surface plays a significant role in LIDA) using a 100 mm focal length, plano-convex CaF_2 lens mounted on a three-axis translation stage system with tip-tilt adjustment (Fig. 1). The sample could be translated out of the beam path, allowing the focal spot to be imaged with a MIR camera (DataRay, WinCamD-FIR2-16-HR). Single pulses were selected with a mechanical shutter and monitored using a beam sampler together with a PbSe photodiode. The single-shot energy was recorded by calibrating this photodiode with an energy meter, while a series of optical filters in conjunction with a waveplate-polarizer attenuator was used to control the pulse energy. This allowed for the on-surface intensity to be determined, which was chosen to account for small variations in the pulse duration at each wavelength. Throughout this Letter, all reported intensities are the peak, on-surface values. A collection of at least 10 laser shots was taken at each energy selected by the attenuator; the sample was translated to a damage-free region for every laser shot. The energy of each individual shot was monitored and recorded. Each damage site was examined under a scanning electron microscope (SEM), and select damage sites were examined

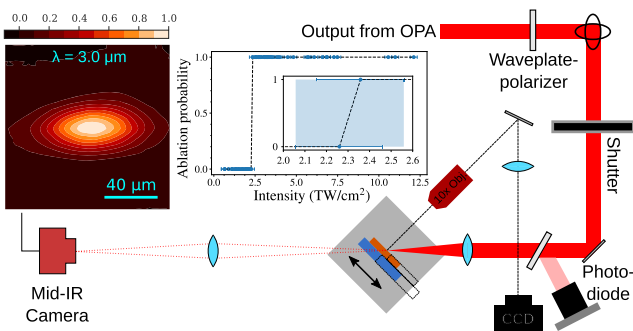


Fig. 1. Experimental setup. Single, MIR pulses were focused onto the Ge sample at a 45° angle of incidence. The sample was mounted on a two-axis translation stage, allowing it to be removed from the beam path. This allowed for direct imaging of the focal spot profile using a MIR camera (an example profile at $\lambda = 3.0\ \mu\text{m}$ is shown). Also shown is the single-shot ablation probability versus intensity for $\lambda = 2.0\ \mu\text{m}$, *s*-polarized light. An abrupt transition is apparent $2.3\ \text{TW}/\text{cm}^2$, corresponding to the ablation threshold (inset: zoom-in of the transition region).

under an atomic force microscope (AFM) to determine whether ablation had occurred.

Ablation was defined as the detectable removal of material beyond the native oxide layer as observed under SEM and confirmed under AFM. Figure 2 shows example damage sites at $2.0\ \mu\text{m}$, $2.4\ \mu\text{m}$, $3.0\ \mu\text{m}$, and $3.6\ \mu\text{m}$ created by single *p*-polarized pulses. SEM analysis revealed that the removed oxide layer always remained partially intact in the vicinity of the corresponding damage site. Analysis under AFM revealed the damage craters to be relatively uniform with a depth of 6–10 nm, confirming not only the removal of oxide (2–3 nm measured by high-resolution TEM), but also the removal of a thin layer of the underlying Ge. For this reason, the type of damage observed here can be considered a weak form of ablation. Examining higher intensity damage sites such as the $8.8\ \text{TW}/\text{cm}^2$ site in Fig. 3 grants insight into the physical mechanism behind the ablation process. Starting at the boundary of the crater, the same type of shallow, uniform ablation observed at lower intensities is present. Moving inward to higher intensities, significant pitting is observed, suggesting the formation of voids after laser excitation. Finally, a transition to a second type of ablation is observed, characterized by a much more erratic surface. Based on this evidence, the first, weaker type of ablation is proposed to be due to the rapid ($<1\ \text{ps}$) melting of a thin surface layer, which has been known to result in the ejection of a top layer of material through a process known as photomechanical spallation [21,22]. This ejected layer would then carry the oxide layer along with it, which is itself observed to remain solid at lower intensities,

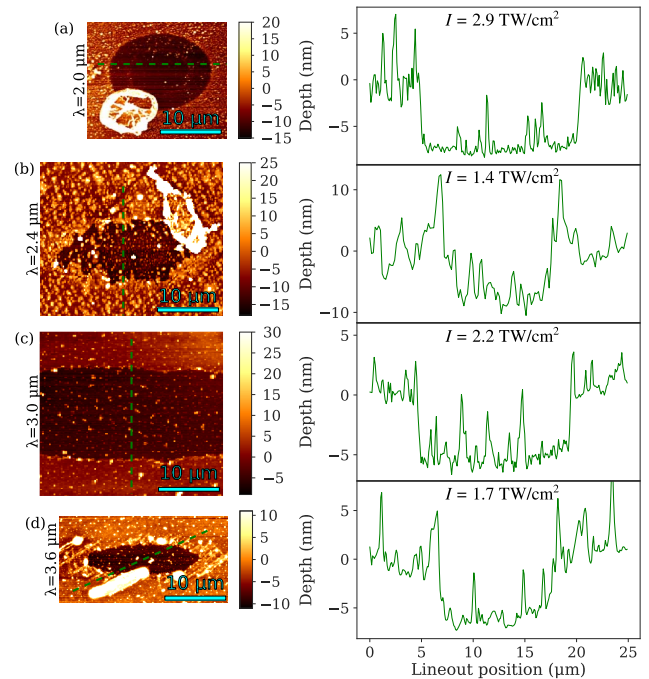


Fig. 2. AFM images (with corresponding lineouts and intensities) of damage/ablation sites from single, *p*-polarized, MIR pulses with $\lambda = 2.0\ \mu\text{m}$, $2.4\ \mu\text{m}$, $3.0\ \mu\text{m}$, and $3.6\ \mu\text{m}$ (a)–(d). Damage sites for $\lambda = 0.78\ \mu\text{m}$ pulses appear very similar to (a). The bright features with raised heights visible in the vicinity of damage sites in (a), (b), and (d) appear to be the semi-intact oxide layer removed from respective sites. As these features are $\sim 100\ \text{nm}$ tall, the maximum height on the color scale has been adjusted to improve visibility.

likely due to the greater melting point and band gap of germanium dioxide. The formation of voids suggests that, at higher intensities, the melted layer begins to boil. At the highest intensities, the critical temperature is reached, leading to the explosive release of vapor in a process known as phase explosion [23]. This is the more erratic type of ablation observed at the center of the damage spot where the intensity is the highest. However, throughout this Letter, the emphasis will be on the weaker, “spallative” type of ablation.

From these images, the ablation threshold was determined by the intensity at which the ablation probability transitioned from 0% to 100%. This is shown in Fig. 1, where the probability of ablation is plotted as a function of intensity for $\lambda = 2.0 \mu\text{m}$, s -polarized light as a representative example. The inset shows a zoom-in of the transition region with the shaded region representing the range of values at which ablation is possible. Figure 4 shows the resulting ablation thresholds for all wavelengths and polarizations. The sources of error in these measurements were the step-size of the intensity scan as well as the uncertainty in the focal spot size and the laser energy.

With this measurement of ablation threshold extending into the MIR, the wavelength dependence of existing theoretical models can be tested. These models make varying assumptions about the excitation of electrons within the material and how this excitation leads to material removal. This results in varying predictions of the ablation threshold, including its dependence on wavelength.

One such model for fs laser-induced ablation is introduced by Gamaly *et al.* [13]. At threshold intensities, Gamaly *et al.* argue based on ionization rates that the conduction band electron density N_{CB} should easily reach and saturate at atomic density N_a . These electrons can then escape from the solid surface and, with sufficient energy, pull ions along with them. By assuming that $N_{\text{CB}} = N_a$ is achieved early in the pulse, the calculations are greatly simplified, allowing for the energy absorbed by the electrons to be determined from simple Fresnel absorption (generalized to arbitrary angle of incidence and polarization for this work). The criterion for ablation to occur is based on the energy absorbed by the electrons: once the average electron energy is sufficient to remove a single ion from the lattice after overcoming the ionization potential, ablation will occur. However, using the ionization potential for this calculation is not reasonable, as it neglects the influence of the rest of the lattice. Instead, it is necessary to use the band gap together with the electron affinity, the energy needed for an electron to transition from the bottom of the conduction band

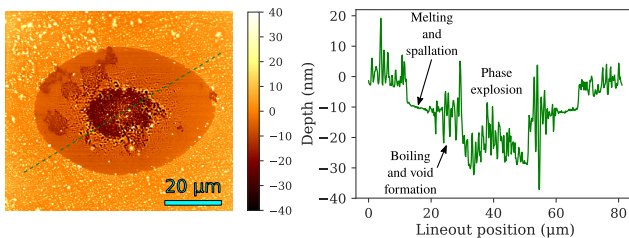


Fig. 3. AFM image and depth profile lineout of a site irradiated by a single $\lambda = 2.0 \mu\text{m}$, p -polarized pulse with an intensity of $8.8 \text{ TW}/\text{cm}^2$, far above the ablation threshold. The profile shows a shallow (10 nm deep) outer crater surrounding a deeper inner crater (30 nm deep). The presence of pits (as deep as 40 nm) in both regions is strong evidence of void formation.

to vacuum, which has been adopted in this work as a modification to the original reference.

While the wavelength dependence of this model has been compared to experimental data for fused silica from the visible regime to the NIR [13], it has never been compared to experimental data in the MIR, where the fundamental assumptions of the model can be tested. For example, it predicts an approximately linear-scaling of the ablation threshold with wavelength due to the increase in skin depth, thereby requiring T_e to be raised for a larger volume of material as wavelength increases. This linear dependence can be seen in Fig. 4(a) (dashed curve). It should be noted that the slope of this scaling is significantly greater than what has been observed experimentally.

Another popular approach in predicting short-pulse laser damage in solids is to apply the Keldysh model of photoionization [24] to non-metal crystals [25–27]. In contrast to the Gamaly model, this model treats the excitation of electrons more thoroughly by considering the transition rate of electrons from a single valence band to the conduction band in the presence of a strong optical field. The electron density in the conduction band can therefore be calculated and compared to a criterion for when ablation is predicted to occur. Additionally, rather than using a material-based criterion (as in the case of the Gamaly model), the optical-based criterion of plasma critical density is typically used [25], which is defined as the value of N_{CB} at which the plasma frequency is equal to the laser frequency. At this electron density, the material is considered metallic, allowing for the subsequent absorption of large amounts of laser energy and, consequently, the onset of material damage.

Simulations were performed using this model of Keldysh ionization, integrating over a 100 fs FWHM pulse envelope to determine the conduction band electron density at the end of the pulse while including the effects of Fresnel reflection at a 45° angle of incidence [solid curve in Fig. 4(a)]. This was done in the NIR to MIR wavelength range, using the critical density as the criterion for ablation. Changes in the refractive

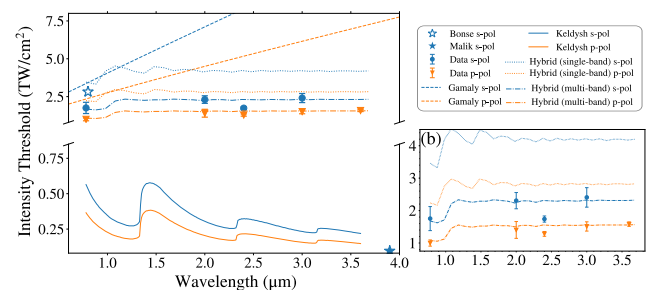


Fig. 4. (a) Experimental single-shot damage/ablation intensity threshold versus wavelength in Ge for both p - and s -polarization light. For comparison, the single-shot melting threshold at $0.8 \mu\text{m}$, with 130 fs pulses [17] and multi-shot damage threshold at $3.9 \mu\text{m}$ with 255 fs pulses [19] are shown as well. The former was performed on a heavily p -doped sample as opposed to the high purity, undoped sample used in this work. This is likely the cause of the discrepancy between the two measurements. Also plotted are the predicted thresholds from Gamaly’s model and the standard application of the Keldysh model to laser damage, i.e., the onset of damage upon reaching plasma critical density. A modification to the latter model was made by including the contributions from all valence bands in Ge and by using the onset of ultrafast melting as the criterion for ablation. For comparison, single-band results are also shown. (b) Zoom-in of the data points in (a).

index due to the generation of free-carriers were not included, and only direct transitions at the Γ point were considered, as calculations of phonon-assisted indirect transition rates did not show a significant contribution to the overall ionization rate. The simulation results show a general decreasing trend with peaks corresponding to channel closure, i.e., an increase in the number of photons needed for ionization. This decreasing trend is due to the choice of critical density as the criterion for ablation: as the wavelength increases, the critical density decreases, allowing the criterion to be reached more easily despite the decreasing photon energy. With this choice of criterion, the predicted thresholds significantly underestimate the ablation threshold.

As neither of the two models is able to explain the wavelength variation of the experimental data, a hybrid model is proposed instead. It continues to treat the excitation of electrons using Keldysh rates, but consists of modifications to the standard Keldysh LIDT model. The first modification was to include the transition contributions from three valence bands (heavy hole, light hole, and split-off bands) with corresponding effective masses [28]. This was necessary, as all three valence bands are comparable in energy near the Γ point, allowing for a greater number of transitions across the band gap. No other changes in the treatment of the electron excitation were included. The second modification was to use a material-based criterion for ablation (as in the Gamaly model) in place of the wavelength-dependent plasma critical density criterion. This criterion was defined as $N_{CB} = 10^{22} \text{ cm}^{-3}$ ($\sim 7\%$ total ionization), which has been identified both theoretically [29] and experimentally [30] as an approximate threshold for the ultrafast melting of semiconductors due to bond softening/weakening. This choice of criterion was motivated by the proposed ablation mechanism of photomechanical spallation as well as the experimental observation of ultrafast melting in Ge [18] after exposure to $0.62 \mu\text{m}$ wavelength, 120 fs pulses at intensities similar to those reported here. Additionally, their reported change in probe reflectivity during exposure to the pump pulse was reported to be at most 10%, suggesting that the approximation of a constant refractive index is not unreasonable. The predictions of this model for the ablation threshold of Ge are shown in Fig. 4 (dotted-dashed curve). A comparatively good agreement with the experimental data was found across all wavelengths. Additionally, this model gives insight into the nature of the wavelength scaling: at shorter wavelengths, the ionization regime is primarily multi-photon. In the MIR, however, there is a transition to tunnel ionization. In this regime, the ionization is primarily field-driven with the effects of channel closure less significant, resulting in a weaker dependence on the photon energy. Further improvements to this simple model can still be made, such as the dynamic variation of the refractive index throughout the pulse.

To summarize, the single-shot, fs-LIA threshold of Ge was measured from NIR to MIR wavelengths, exhibiting a weak type of ablation in which the native oxide layer was removed along with nanometers of the underlying Ge. This process is believed to be due to the ultrafast melting of a surface layer of Ge, ultimately leading to photomechanical spallation. As the measured damage thresholds disagree with two popular theoretical models, a hybrid multi-band model is proposed in which the onset of ablation coincides with the occurrence of ultra-fast melting. This model agrees well with data, offering a means by which the fs-LIDA threshold of other

semiconductors may be estimated over a large range of wavelengths.

Funding. Air Force Office of Scientific Research (AFOSR) (FA9550-16-1-0069, FA9550-16-1-0013); National Science Foundation (NSF) (1605042).

REFERENCES

- H. Pires, M. Baudisch, D. Sanchez, M. Hemmer, and J. Biegert, *Prog. Quantum Electron.* **43**, 1 (2015).
- A. V. Mitrofanov, A. A. Voronin, D. A. Sidorov-Biryukov, A. Pugžlys, E. A. Stepanov, G. Andriukaitis, T. Flöry, S. Ališauskas, A. B. Fedotov, A. Baltuška, and A. M. Zheltikov, *Sci. Rep.* **5**, 8368 (2015).
- D. Haberberger, S. Tochitsky, and C. Joshi, *Opt. Express* **18**, 17865 (2010).
- S. Ghimire, A. D. DiChiara, E. Sistrunk, P. Agostini, L. F. DiMauro, and D. A. Reis, *Nat. Phys.* **7**, 138 (2010).
- A. E. Dormidonov, V. O. Kompanets, S. V. Chekalin, and V. P. Kandidov, *Opt. Express* **23**, 29202 (2015).
- R. Soref, *Nat. Photonics* **4**, 495 (2010).
- L. Zhang, A. M. Agarwal, L. C. Kimerling, and J. Michel, *Nanophotonics* **3**, 247 (2014).
- M. P. Fischer, C. Schmidt, E. Sakat, J. Stock, A. Samarelli, J. Frigerio, M. Ortolani, D. J. Paul, G. Isella, A. Leitenstorfer, P. Biagioni, and D. Brida, *Phys. Rev. Lett.* **117**, 047401 (2016).
- R. Adato, A. A. Yanik, J. J. Amsden, D. L. Kaplan, F. G. Omenetto, M. K. Hong, S. Erramilli, and H. Altug, *Proc. Natl. Acad. Sci. USA* **106**, 19227 (2009).
- F. K. Tittel, D. Richter, and A. Fried, *Solid-State Mid-Infrared Laser Sources* (Springer, 2003), pp. 458–529.
- A. H. Nejadmalayeri, P. R. Herman, J. Burghoff, M. Will, S. Nolte, and A. Tünnermann, *Opt. Lett.* **30**, 964 (2005).
- B. N. Chichkov, C. Momma, S. Nolte, F. Von Alvensleben, and A. Tünnermann, *Appl. Phys. A* **63**, 109 (1996).
- E. G. Gamaly, A. V. Rode, B. Luther-Davies, and V. T. Tikhonchuk, *Phys. Plasmas* **9**, 949 (2002).
- D. M. Simanovskii, H. A. Schwettman, H. Lee, and A. J. Welch, *Phys. Rev. Lett.* **91**, 107601 (2003).
- D. R. Austin, K. R. P. Kafka, S. Trendafilov, G. Shvets, H. Li, A. Y. Yi, U. B. Szafruga, Z. Wang, Y. H. Lai, C. I. Blaga, L. F. DiMauro, and E. A. Chowdhury, *Opt. Express* **23**, 19522 (2015).
- D. R. Austin, K. R. P. Kafka, Y. H. Lai, Z. Wang, K. Zhang, H. Li, C. I. Blaga, A. Y. Yi, L. F. DiMauro, and E. A. Chowdhury, *J. Appl. Phys.* **120**, 143103 (2016).
- J. Bonse, G. Bachelier, J. Siegel, and J. Solis, *Phys. Rev. B* **74**, 1 (2006).
- K. Sokolowski-Tinten, A. Cavalleri, and D. Von der Linde, *Appl. Phys. A* **69**, 577 (1999).
- R. Malik, B. Mills, J. H. V. Price, M. Petrovich, Z. Muktadir, Z. Li, and H. N. Rutt, *Appl. Phys. A* **113**, 127 (2012).
- M. Wu, D. A. Browne, K. J. Schafer, and M. B. Gaarde, *Phys. Rev. A* **94**, 063403 (2016).
- D. von der Linde and K. Sokolowski-Tinten, *Appl. Surf. Sci.* **154–155**, 1 (2000).
- T. Kumada, T. Otobe, M. Nishikino, N. Hasegawa, and T. Hayashi, *Appl. Phys. Lett.* **108**, 011102 (2016).
- P. Lorazo, L. J. Lewis, and M. Meunier, *Phys. Rev. Lett.* **91**, 225502 (2003).
- L. V. Keldysh, *Sov. Phys. JETP* **20**, 1307 (1965).
- B. C. Stuart, M. D. Feit, S. Herman, A. M. Rubenchik, B. W. Shore, and M. D. Perry, *Phys. Rev. B* **53**, 1749 (1996).
- V. E. Gruzdev, *J. Opt. Technol.* **71**, 504 (2004).
- P. Balling and J. Schou, *Rep. Prog. Phys.* **76**, 036502 (2013).
- V. Gruzdev, D. R. Austin, O. N. Sergaeva, and E. Chowdhury, *CLEO: Science and Innovations* (Optical Society of America, 2017), paper STh4J-6.
- P. Stampfli and K. H. Bennemann, *Phys. Rev. B* **42**, 7163 (1990).
- C. W. Siders, A. Cavalleri, K. Sokolowski-Tinten, C. Toth, T. Guo, M. Kammler, M. H. Von Hoegen, K. R. Wilson, D. von der Linde, and C. P. Barty, *Science* **286**, 1340 (1999).